Materials & Design 184 (2019) 108184

Contents lists available at ScienceDirect

Materials & Design

journal homepage: www.elsevier.com/locate/matdes

Fracture behavior of multilayer fibrous scaffolds featuring microstructural gradients

W Khoo [a], SM Chung [a], Shing Chee Lim [a], Cheng Yee Low [a], Jenna M. Shapiro [b], Ching Theng Koh [a, *]

[a] Faculty of Mechanical and Manufacturing Engineering, University of Tun Hussein Onn Malaysia, Johor, Malaysia
[b] Faculty of Engineering, University of Bristol, Bristol, United Kingdom

HIGHLIGHTS

- Bioinspired nanofibrous gelatin scaffolds featuring fiber density gradients were fabricated *via* an electrospinning process.
- A finite element model was developed to examine inhomogeneous stress distribution of graded fibrous networks at a notch root.
- Microstructural gradients resulted in corresponding gradual changes of properties over the thickness of the scaffold.
- Gradients in both network density and fiber alignment increased the toughness of the graded fibrous scaffolds in simulations.

GRAPHICAL ABSTRACT

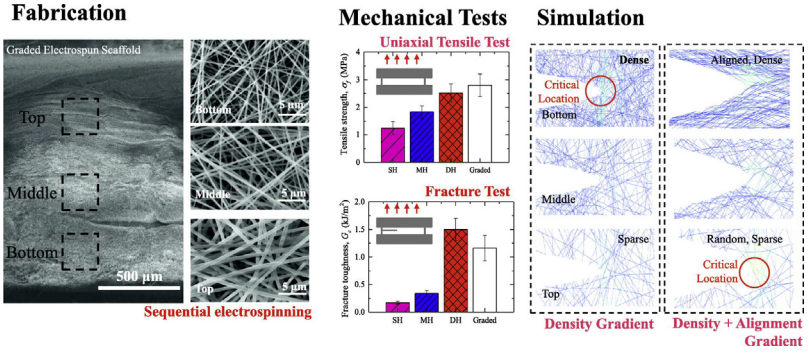

ARTICLE INFO

Article history:
Received 18 June 2019
Received in revised form
2 September 2019
Accepted 3 September 2019
Available online 4 September 2019

Keywords:
Functionally graded materials
Multilayer fibrous scaffolds
Electrospinning
Tissue engineering
Finite element analysis
Mechanical properties

ABSTRACT

Multilayer nanofibrous scaffolds that mimic the microstructure gradient of connective tissues have shown promising results in tissue regeneration, but the effect of these gradients on the mechanical performance of fiber meshes is poorly understood. In this study, trilayer nanofibrous gelatin scaffolds with gradually increasing fiber diameters (227–679 nm) and pore sizes (1.14–4.93 μm^2) were fabricated using a sequential electrospinning process, producing a fiber density gradient over the scaffold thickness. The mechanical properties of the fibrous scaffolds were evaluated using uniaxial tensile and fracture tests. Deformation of microscopic crack tip openings was simulated using finite element analysis. Results from uniaxial and fracture tensile tests showed that the mechanical properties of fibrous scaffolds were governed by network architectures. The microstructure gradient yielded corresponding changes of material properties over the scaffold thickness. Simulation results showed different stress distribution and energy dissipation at each layer of the graded scaffolds. Finite element analysis also revealed that a combination of network density and alignment gradients can improve fracture toughness of graded scaffolds. This study provides guidelines and methodologies for designing tailored gradient fibrous scaffolds to more closely mimic the structural and mechanical properties of native interfacial tissues.

* Corresponding author.
E-mail address: ctkoh@uthm.edu.my (C.T. Koh).

https://doi.org/10.1016/j.matdes.2019.108184

1. Introduction

Multilayered fibrous structures have a variety of functions in multiple applications, ranging from filtration, to textiles, to tissue engineering. In filtration, multilayer structures affect pressure drop and dust holding efficiency [1,2]. Multilayer fibers in textiles can act as an acoustic absorption material to reduce noise [3]. Further, multilayer fibrous materials are used as tissue engineering scaffolds to provide suitable microenvironments for cells to support the repair and regeneration of injured tissues.

Microstructural and compositional gradients have been found in several interface tissues, such as ligament-to-bone [4], tendon-to-bone [5] and cartilage-to-bone [6]. These gradients play important roles in transmitting loads from soft to hard tissues [7–9]. Variations in extracellular matrix composition and microstructural architecture were also found in connective tissues, including cartilage [10]. In cartilage, this variation leads to directional stiffness characteristics and inhomogeneous distribution of strain [11,12].

Due to their importance in the performance of biomechanical functions, gradient structures have inspired design of biomimetic tissue engineered scaffolds. Methods to produce scaffolds with gradient structures include additive manufacturing/3D printing [13], iterative layered freeze-drying processes [14], and electrospinning [15,16]. Gradients are achieved through the development of microstructural architectures, which vary across the scaffold thickness. This includes varying pore sizes [17], fiber alignment and orientation, chemical composition [18] and combinations of these properties [19].

Functionally graded scaffolds with thickness-dependent microstructural architectures mimic the native microenvironment and provide instructive cues for cell growth and regeneration. Implementation of these biomimetic graded scaffolds in both *in vitro* and *in vivo* studies indicated promising results for directing cell fate and tissue regeneration. Graded scaffolds were found to improve cell differentiation [20], seeding efficiency, and cell distribution [21] as compared to homogeneous scaffolds. Gradient microstructures were also used as a template to guide cell organization [22] and transportation of both nutrients and cells [16].

While *in vitro* and *in vivo* applications of functionally graded scaffolds have been extensively studied, there is still an incomplete understanding of the mechanical behavior of graded scaffolds. Bilayer electrospun membranes have been shown to possess a larger modulus and improved fracture properties compared to single layered membranes [23]. Multilayered electrospun scaffolds with gradient structures eliminated anisotropic strain properties and resulted in a mechanically integrated unified fracture [24]. Most studies on the mechanical evaluation of fibrous scaffolds have been based on homogeneous systems [25,26]. Finite element simulation of two dimensional micromechanical fibrous networks on short fibers [27] and long fibers [28,29] demonstrated that elastic modulus of the networks was dependent on their microstructural architectures, including fiber diameter, density and inter-fiber bonding. In addition to microstructural architecture, fiber properties, including gel strength, also influence scaffold properties [25,30–34].

This study investigates the effect of varying microstructural morphologies, in particular fiber diameter, fiber density and fiber alignment, on the mechanical properties of graded nanofibrous scaffolds. We hypothesize that multilayer graded scaffolds will exhibit improved fracture behavior as compared to homogeneous materials, which can then be used to prevent mechanical mismatch and discontinuity at tissue interfaces. Ultimately, our aim is to better understand the design and fracture behavior of graded scaffolds using experimental and computational methods to inform rational design of scaffolds for interfacial and connective tissue engineering.

Functionally graded trilayer scaffolds with gradually increasing fiber diameter (~200 to ~700 nm) were produced by varying process parameters in a sequential electrospinning technique. Homogeneous scaffolds, featuring similar microstructural architectures to individual layers of the graded scaffold, were fabricated to serve as a basis of comparison for morphological characterization and for mechanical testing. Uniaxial tensile and fracture tests were conducted and fracture mechanisms of the homogeneous and graded scaffolds were observed. Computational finite element analysis of the microscopic fracture at the crack tip of three dimensional graded fibrous scaffolds was performed. Microstructural architecture variations, including gradients in network density and fiber alignment, were also simulated to provide future design guidelines for functionally graded scaffolds.

2. Materials and methods

2.1. Experimental section

2.1.1. Sample preparation

A 25 wt% solution of cold water fish skin gelatin with a molecular weight of 60 kDa (Sigma Aldrich, USA) in a mixture of 90 wt% glacial acetic acid (Merck, Germany) and 10 wt% water was prepared. The gelatin solution was stirred overnight at room temperature before loading into a 50 mL plastic syringe (Terumo, UK) in our bespoke electrospinning apparatus. The solution was pumped through a blunt 23 gauge needle (Terumo, UK) at a constant feed rate by a syringe pump (KD Scientific, USA). A voltage was supplied between the needle and a grounded metal collector using a high voltage power supply (Glassman, UK) to produce nanofibers.

A sequential electrospinning process was used to produce functionally graded scaffolds consisting of distinct trilayer microstructures. For each layer, electrospinning process parameters of voltage, feed pump rate, working distance, and deposition time were varied. In the first step, operating parameters were set to voltage $V = 9$ kV, pump rate $f = 0.15$ ml/h and distance $d = 20$ cm. After 30 h of electrospinning, the machine parameters were then adjusted to $V = 15$ kV, $f = 0.3$ ml/h and $d = 20$ cm for the second step. After 6 h of the electrospinning process, the machine parameters were finally adjusted to $V = 15$ kV, $f = 0.45$ ml/h and $d = 15$ cm for the third step. The process was completed after 45 min of electrospinning.

In order to compare mechanical properties of the individual layers, three homogeneous scaffolds were also fabricated. Homogeneous scaffolds with densely packed fibers (DH) were fabricated using the parameters of the first step of the sequential process. Homogeneous scaffolds with moderately packed fibers (MH) were fabricated using the second step process parameters. Homogeneous scaffolds with sparsely packed fibers (SH) were fabricated using the third step parameters for 2 h, rather than 45 min. Eight to twelve samples were prepared from each type of scaffold for tensile and fracture tests. The thickness for each sample was measured three times using digital calipers (Facom, France). The thicknesses of graded, DH, MH and SH scaffolds were 0.56 ± 0.13, 0.16 ± 0.04, 0.34 ± 0.05 and 0.33 ± 0.06 mm, respectively.

2.1.2. Morphology characterization and quantification

Cross-sectional and top-view morphologies of the graded scaffolds were observed *via* scanning electron microscopy (SEM, Hitachi, USA). To observe the morphology of each layer, samples were prepared by cutting squares of approximately 10 mm × 10 mm from the scaffold after each step of the electrospinning process. To observe the cross-sectional morphology, following the completion

of the sequential electrospinning process, the graded scaffold was cut across its thickness using a scalpel and visualized using SEM.

All samples were gold coated before SEM observation at an accelerating voltage of 10 kV. The network morphology, including fiber diameters, pore sizes and fiber orientation of each layer, were quantified using image analysis software ImageJ (NIH, Bethesda, MD, USA) [35]. For pore size measurement, the SEM images were first converted to black and white. The area of the void space between fibers was measured as pore size, using the measuring tool in ImageJ. The average fiber diameters and pore sizes were determined by measuring and averaging the diameters of ten randomly chosen fibers and pore sizes respectively from one SEM image for each type of scaffold.

2.1.3. Uniaxial and fracture tests

Uniaxial tensile and fracture tests were performed on both functionally graded scaffolds and homogeneous scaffolds using a universal testing machine (Lloyd Instruments Ltd., UK). A 10 N load cell was used for homogeneous scaffolds, which experienced forces up to 8.5 N. Functionally graded scaffolds experienced forces up to 46 N, necessitating the use of a 500 N load cell. Scaffolds for both tests were cut into a rectangular shape of 24 mm in width and 3 mm in height. For fracture test samples, a notch with 8 mm length was introduced at the center of the sample, perpendicular to the loading direction. The test samples were gripped along their width and separated at constant speed of 3 mm/min until failure. Four to six samples were tested for each tensile and fracture test.

The tensile strength σ_f, fracture strain ε_f, and elastic modulus E were measured from the uniaxial test. The tensile strength, σ_f, was the maximum stress value in the stress-strain response. The fracture strain, ε_f, was the strain corresponding to the tensile strength. The elastic modulus, E, was determined from the slope of the linear region of the stress-strain curves, between $\varepsilon = 0.1$ and $\varepsilon = 0.15$. The fracture toughness, G_c, was determined following the method described by Rivlin and Thomas [36]. G_c was calculated using Eq. (1):

$$G_c = W_o l_o \tag{1}$$

The elastically stored energy per unit volume, W_o, was determined from the area under the stress-strain curve of the uniaxial test sample, up to the fracture strain, ε_f, of fracture samples. The initial distance between the clamps, l_o, is the height of uniaxial test samples.

The fracture surface of the crack tip was examined following the method developed by Koh et al. [37]. The samples were stretched on the universal testing machine to the assigned engineering strains of $\varepsilon_1 = 0.11$, $\varepsilon_2 = 0.29$, and $\varepsilon_3 = 0.33$, which were informed by the results of the fracture testing. The sections of the deformed samples containing the crack tips were then affixed to adhesive tape and visualized by SEM.

2.1.4. Statistical analysis

Results are expressed as mean ± standard deviation. Statistical analysis was conducting using one-way ANOVA analysis and Fisher's test. A p value of <0.05 was considered to be statistically significant.

2.2. Computational analysis

2.2.1. Finite element modeling

Meshes were generated using MATLAB (Version 2017, MathWorks, Natick, MA, USA). Finite element analysis was performed with Abaqus (Version 2017, SIMULIA, Providence, RI, USA). Models were constructed by depositing fibers in separate x-y planes in a three-dimensional circular unit model. These fibers were placed at random locations, with a slope m following the user-defined angles Θ (Fig. 1). The defined angle Θ represents the alignment of the fibers and generates random lines inclined from negative to positive slopes (Eq. (2)).

$$tan(-\theta) < m < tan(\theta) \tag{2}$$

The models had the first layer ($i = 1$) placed at $z_1 = 0$. Consecutive layers were placed in a separate plane at $z_{i+1} = z_i + \Delta z$, with offset distance Δz from the previous layer. The offset distance was determined from the sum of fiber radii of both adjacent layers.

Random fibers were crosslinked by assigning the same nodes at the intersection points. Two types of crosslinking modeled in this work include intralayer crosslinking, where 15% of the intersection points on each layer were randomly crosslinked, and interlayer crosslinking, where 15% of the intersection points of fibers located on two adjacent layers were randomly crosslinked. Fiber density, ρ_f, was defined as the sum of fiber length per unit area, and was calculated using MATLAB.

Both density and alignment gradient models were studied in this paper, involving the construction of three types of graded networks: density graded (DG), alignment graded (AG), and density and alignment graded (DAG) networks. Homogeneous multilayer networks were also modeled. The DG networks have density gradually reduced over the network thickness. The density gradient was quantified as the percentage fiber density change between fibrous networks located on two consecutive layers. The AG networks had fiber orientation gradually changed over the network thickness. The DAG networks had both density and alignment changed over the thickness.

Fibrous network models were constructed with two levels of fiber density (Table 1). The number of fiber N was assigned to randomly generate fibers in a circular unit of fibrous network. The value of fiber density ρ_f was then determined from the networks in MATLAB. The first level of fiber density ranged from 6.6 to 6.8 μm^{-1} while the second level ranged from 67 to 68 μm^{-1}. The DG networks were constructed with gradients ranging from 10% to 58%. Alignment angles were assigned from 15° to 90° at each layer in AG and DAG networks. All case studies were repeated three times to account for the stochastic nature of the fibrous networks.

Meshes generated from MATLAB were imported into the finite element software, Abaqus. Fibers were modeled with Timoshenko beam (B31) and were analyzed using nonlinear finite element analysis, which considers large strain and rotation. All fibers were defined with diameter Ø of 300 nm, Young's modulus, E, of 100 MPa and fracture strength, σ_f, of 30 ± 4 MPa.

2.2.2. Fracture analysis

Detailed deformation of the fibrous microstructure around the crack tip was modeled by constructing fibrous networks in a circular unit (radii ranging from 5 to 75 μm) with a notch length corresponding to the unit radius. All nodes located on the perimeter of the circle were assigned with displacements u_1 and u_2 (Eqs. (3) and (4)), which are associated with the macroscopic crack tip field for homogeneous and isotropic materials. The applied displacements were calculated from the classical equations of linear elastic fracture mechanics [38]:

$$u_1 = \frac{1}{2}\sqrt{\frac{r}{2\pi}}\,\frac{K_I}{G}\left[\kappa - 1 + 2sin^2\frac{\Theta}{2}\right]cos\frac{\Theta}{2} \tag{3}$$

$$u_2 = \frac{1}{2}\sqrt{\frac{r}{2\pi}}\,\frac{K_I}{G}\left[\kappa + 1 - 2cos^2\frac{\Theta}{2}\right]sin\frac{\Theta}{2} \tag{4}$$

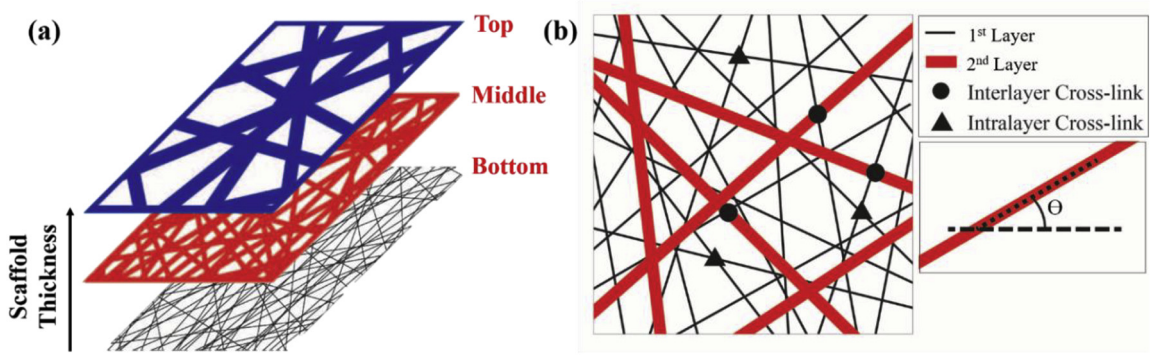

Fig. 1. Schematic illustration of (a) experimentally produced graded electrospun scaffolds and (b) finite element model for density graded fibrous networks.

Table 1
The network parameters of homogeneous (H), density graded (DG), alignment graded (AG) and density and alignment graded (DAG) networks.

Network name	Fiber density, $\rho_{f\ (1st\ layer)}$ (μm^{-1})	Density gradient, G (%)	Fiber alignment, Θ (°)	Model size, r (μm)	Fiber number, $N_{(1st\ layer)}$
H1	6.8 ± 0.1	0	90	75	1170
H2	68.5 ± 0.9	0	90	5	800
DG1	6.7 ± 0.1	10 ± 2	90	75	1170
	6.7 ± 0.1	18 ± 2	90	75	1170
	6.7 ± 0.2	29 ± 1	90	75	1170
	6.6 ± 0.2	42 ± 2	90	75	1170
	6.6 ± 0.1	50 ± 2	90	75	1170
	6.6 ± 0.2	58 ± 2	90	75	1170
DG2	68.0 ± 0.9	20 ± 3	90	5	800
	67.6 ± 0.3	49 ± 1	90	5	800
AG	67.6 ± 0.9	0	15, 52.5, 90	5	800
DAG	68.0 ± 0.5	13 ± 2	15, 52.5, 90	5	800
	68.3 ± 0.2	29 ± 2	15, 52.5, 90	5	800
	68.0 ± 0.5	50 ± 1	15, 52.5, 90	10	1600

The origin was assigned at the notch root in polar coordinates (r, θ). K_I is the stress intensity factor for mode I. The shear modulus, G, was assigned to be 4 MPa, with a Poisson's ratio, ν, of 0.3, where $\kappa = (3 - \nu)/(1 + \nu)$. The fracture points presented in this paper refer to the crack opening when the first fiber element exceeds its fracture strength.

3. Results

3.1. Morphology of homogeneous and graded electrospun scaffolds

SEM images of graded electrospun scaffolds show the three distinct layers produced by the sequential electrospinning process, which result in changes in microstructural architecture over the sample thickness (Fig. 2). The SEM images of the scaffold cross section taken at high magnification illustrate the gradual decrease in fiber packing density from the bottom to top layer. The microstructural morphology of the graded scaffold layers were compared to the corresponding homogeneous scaffolds: top to SH layers, middle to MH layers and bottom to SH layers. Quantitative image analysis of the top view of the scaffold layers shows that all electrospun fibers were randomly aligned in each layer (Fig. 3).

Further analysis of the top-view images of the graded scaffolds shows that fiber diameter increased from 227 ± 23 nm at the bottom layer, to 394 ± 62 nm at the middle layer and 679 ± 45 nm at the top layer (Fig. 4a). Pore sizes also increased from 1.14 ± 0.28 μm^2 at the bottom layer, to 2.60 ± 1.15 μm^2 at the middle layer and 4.93 ± 2.09 μm^2 at the top layer (Fig. 4b). Statistical analysis shows significant differences in both fiber diameters and pore sizes for the different layers of graded scaffolds. A similar trend was found in homogeneous scaffolds. The fiber diameters of the three types of homogeneous scaffolds were significantly different; fiber diameters increased from 205 ± 15 nm in the DH layer, to 436 ± 70 nm in the MH layer and 739 ± 110 nm in the SH layer (Fig. 4a). The pore size also decreased from 0.74 ± 0.28 μm^2 for DH, to 2.91 ± 1.38 μm^2 for MH and 7.40 ± 3.56 μm^2 for SH (Fig. 4b).

Statistical analyses comparing morphological parameters of the graded scaffold to the homogeneous layers shows that the SH and MH layers were morphologically the same as the top and middle layers of the graded scaffold, respectively. However, fiber diameter and pore size of the DH layer were different from those of the bottom layer of the graded scaffold.

3.2. Mechanical testing on homogeneous and graded electrospun scaffolds

The analysis of the mechanical performance of homogeneous and graded scaffolds is shown in Fig. 5. Graded scaffolds exhibited the largest tensile strength with a mean of 2.80 ± 0.41 MPa, which was significantly different to that of the DH scaffolds. The tensile strength of the SH scaffold was the lowest, with a mean strength approximately half that of the other scaffolds. The graded scaffold showed the largest strain at fracture with a mean of 0.77 ± 0.11, followed by the DH scaffold (ε_f = 0.32 ± 0.08), MH scaffold (ε_f = 0.19 ± 0.04) and SH scaffold (ε_f = 0.14 ± 0.01). In contrast to tensile strength, the graded scaffolds had the smallest elastic modulus with a mean of 9.44 ± 1.88 MPa. The elastic moduli of the SH (13.39 ± 3.02 MPa) and MH scaffolds (14.46 ± 3.16 MPa) were not significantly different. As with tensile strength, the fracture toughness of the graded scaffold (G_c = 1.16 ± 0.23 kJ/m^2) was comparable to the DH scaffold (G_c = 1.50 ± 0.20 kJ/m^2). SH scaffolds had the least fracture toughness of 0.17 ± 0.03 kJ/m^2.

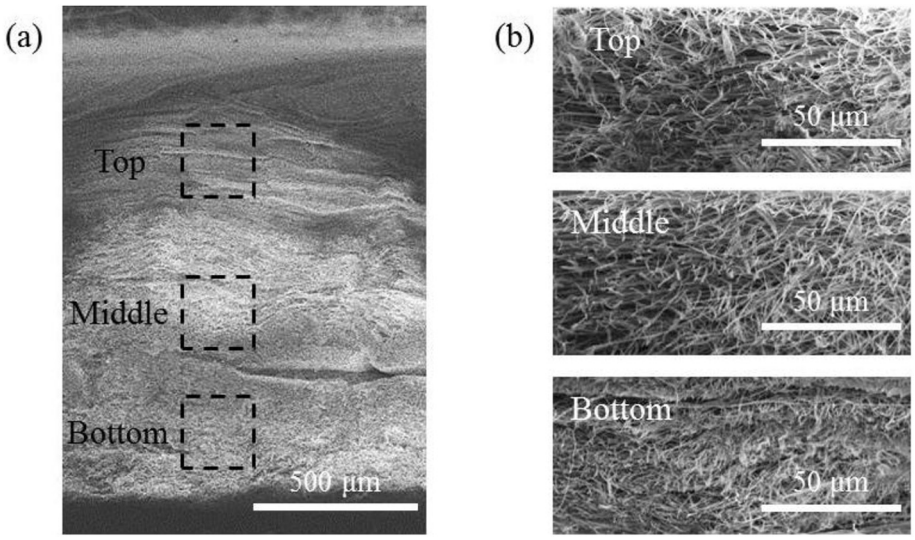

Fig. 2. Microstructural architecture of graded scaffolds. (a) Cross section of graded scaffold. (b) High magnification of the cross section, showing the constituent layers of the graded scaffold, enclosed by rectangular boxes in (a).

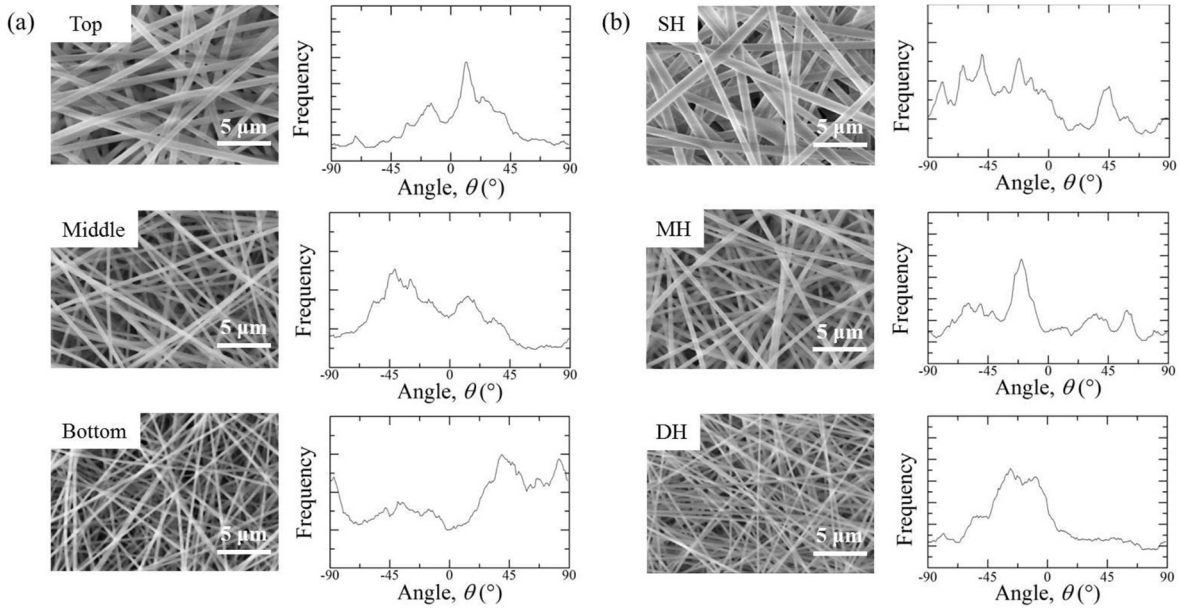

Fig. 3. Morphology and fiber orientation of (a) graded and (b) homogeneous scaffolds.

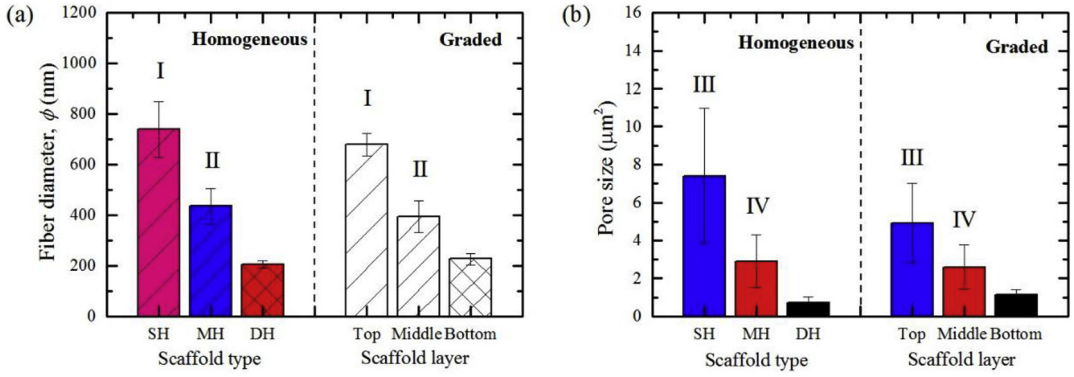

Fig. 4. Quantification of (a) fiber diameter and (b) pore size for homogeneous and each layer in the graded scaffolds. The groups marked with same Roman numerals (I, II, III and IV) are not significantly different ($p > 0.05$).

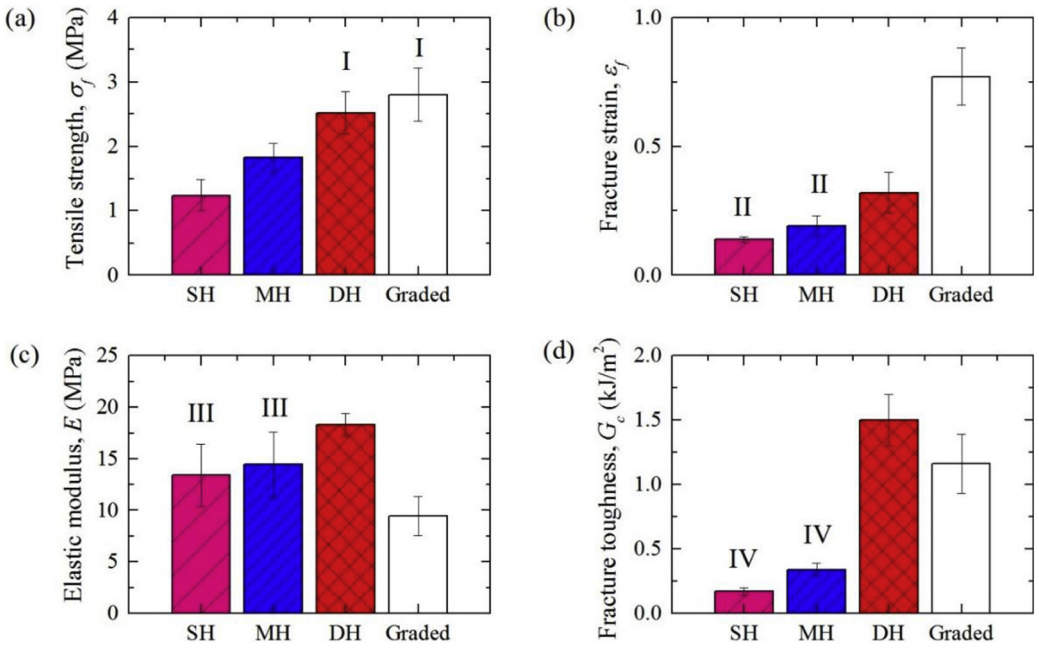

Fig. 5. Mechanical testing of homogeneous and graded scaffolds. (a) Tensile strength, σ_f, (b) fracture strain, ε_f, (c) elastic modulus, E, (d) fracture toughness, G_c of homogeneous and graded scaffolds. The groups marked with same Roman numerals (I, II, III and IV) are not significantly different ($p > 0.05$).

Fig. 6 shows the failure mechanism of graded scaffolds, which was visualized using SEM. The crack of the top layer started to propagate while the notch in the middle and bottom layers blunted at strain ε_1. As the scaffold was further stretched to strain ε_2, the crack of middle and bottom layers also started to propagate across the scaffold. At strain ε_3, the crack of all three layers propagated across the scaffold.

3.3. Design of graded fibrous networks using FEA

Fig. 7 shows the fracture of DG and DAG networks corresponding to various gradients. The network fracture is described by stress intensity factor K, which corresponds to the K-dominant strain field assigned at the boundaries when the first fiber element exceeds its tensile strength. The DG networks have consistent fracture points corresponding to an increase of network density gradient. The stress intensity factor of both H1 and DG1 networks with low fiber density of 6.6–7.8 μm^{-1} increased to more than twice that of the H1 and DG1 networks with 67.6–68.5 μm^{-1} density. In addition to a network density gradient, fiber alignment gradients were incorporated in AG and DAG networks. The AG network had similar fracture behavior to the homogeneous networks with equivalent fiber densities. The DAG networks showed a larger stress intensity as compared to DG networks with similar fiber densities.

The deformation and stress distribution at the crack tip were examined during fracture of homogeneous and graded networks (Fig. 8). The fracture of DG networks occurred at the crack tip of the densest network, which had the largest stress concentration. The fracture point of AG networks, which had similar network density for all layers, was located at the layer comprised of randomly oriented fibers. The fibers in AG networks aligned parallel to the notch dissipate energy by rearranging and realigning fibers perpendicular to the crack tip during crack tip opening. In contrast to DG networks, the fracture of DAG networks occurred at the layer with

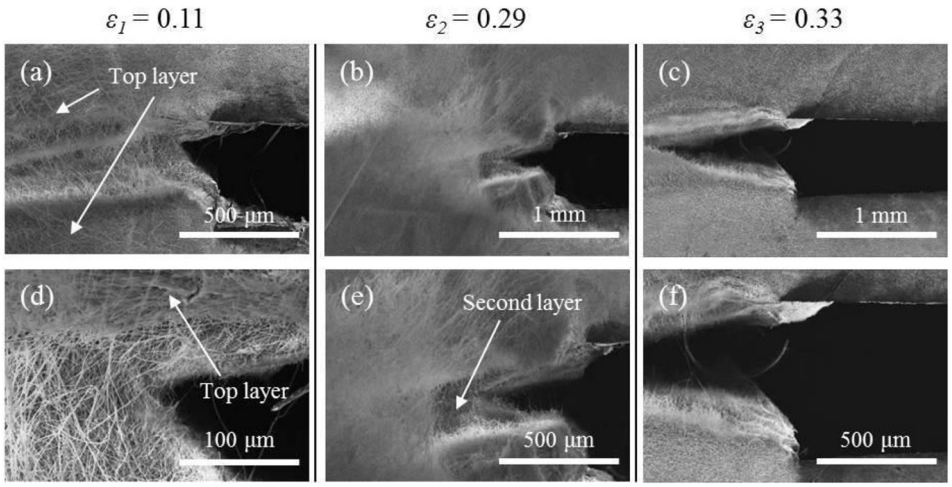

Fig. 6. SEM images of the failure mechanism of graded scaffolds following fracture tests. The scaffold was deformed by strain (a, d) $\varepsilon_1 = 0.11$, (b, d) $\varepsilon_2 = 0.29$ and (c, f) $\varepsilon_3 = 0.33$.

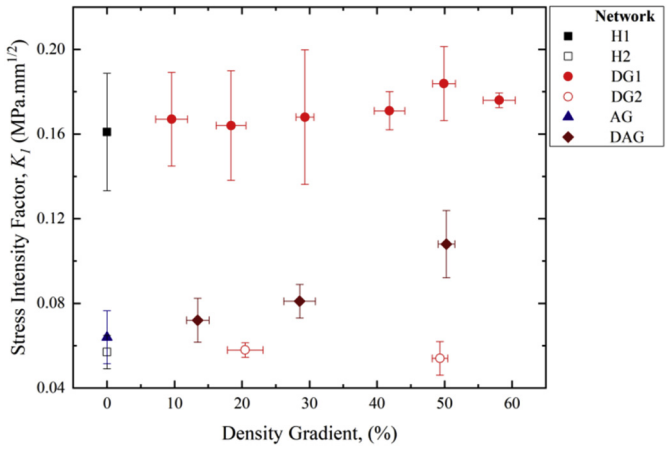

Fig. 7. Stress intensity factor for homogeneous networks, DG networks, AG networks and DAG networks.

sparse fiber density and randomly oriented fibers. In order to encourage more fiber rearrangement and realignment to dissipate energy, aligned fibers were associated with the densest layer of the DAG scaffolds.

4. Discussion

In this paper, we present both experimental and computational methods for producing functionally graded multilayer nanofibrous scaffolds and evaluating their mechanical properties and fracture behaviors. Gelatin was chosen as the scaffold material due to its biodegradability, biocompatibility and ready availability at low cost. Moreover, *in vitro* studies have shown that gelatin promotes cell proliferation [39], adhesion, and infiltration [40].

Trilayer gelatin nanofibrous scaffolds featuring fiber density gradients across their thicknesses were fabricated using a sequential electrospinning method. Shifts from dense to sparse fiber packing and fiber diameter were achieved by altering the electrospinning process parameters. These process parameters included solution feed rate (0.15 ml/h to 0.45 ml/h), needle-to-plate distance (15 cm to 20 cm) and applied voltage (9 kV to 15 kV). However, the chemical composition of the polymer solution (*e.g.* molecular weight and concentration) was maintained throughout the fabrication process to avoid inconsistencies in fiber properties across layers associated with compositional changes [16,24].

Besides fiber diameter and packing density, pore size is another critical parameter in tissue engineering; modulating pore size is important for encouraging cell growth and migration or alternatively, limiting cell motility [41]. Further, pore size is always related to porosity, which contributes to scaffold permeability, enabling transport of nutrients, oxygen and waste [16,42]. Scaffolds constructed with pore size gradient architectures were shown to promote anisotropic cell distribution within the scaffold, similarly to native tissues such as cartilage [43]. Our results also demonstrated a pore size gradient within the scaffolds; we believe such architecture will impact *in vitro* cellular response. However, further studies are needed to investigate the potential of these graded scaffolds in guiding zonal cell and matrix composition.

Homogeneous scaffolds with comparable composition and morphology to corresponding layers of the graded scaffolds were produced and mechanically tested. Uniaxial tensile and fracture tests on homogeneous scaffolds with sparse, moderate and dense networks demonstrate statistically significantly distinctive mechanical properties, including tensile strength and fracture toughness (Fig. 5). The graded scaffolds, constructed of three layers with similarly sparse, moderate and dense networks, were likely to have the local mechanical properties increased over the scaffold thickness, resulting in the observation of layer-by-layer fracture (Fig. 6).

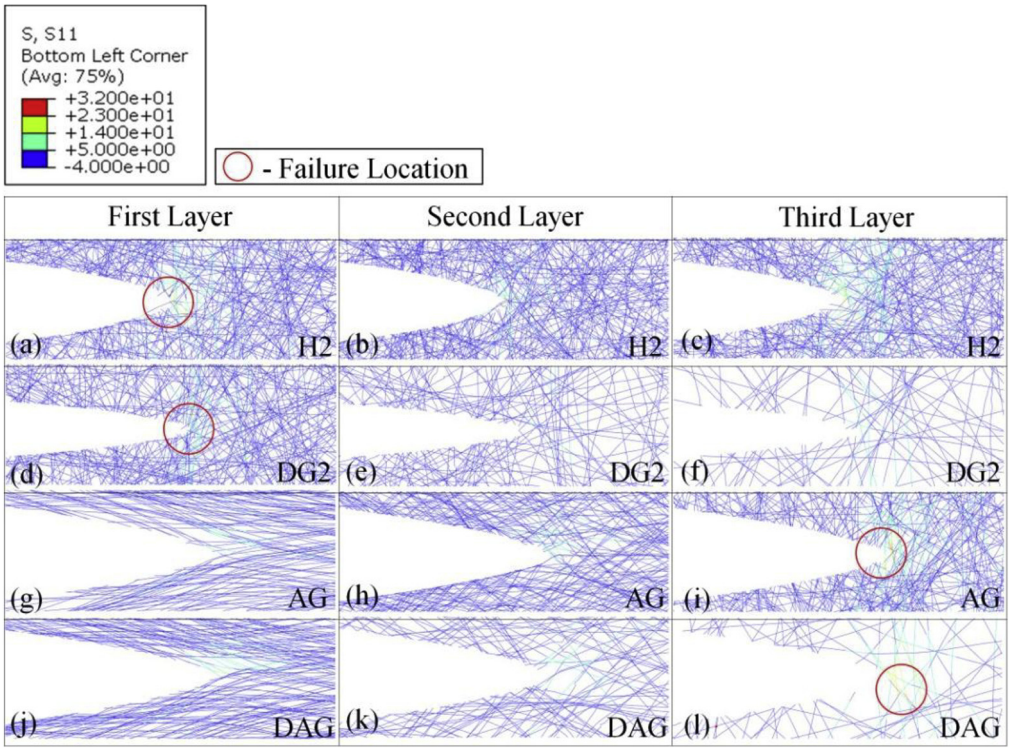

Fig. 8. Comparison of the critical crack opening of homogeneous and graded fibrous networks at first, second and third layers: (a–c) H2 networks, (d–f) DG networks, (g–i) AG networks and (j–l) DAG networks.

The finite element analysis on the microscopic deformation near the crack tip also shows that fibers at each layer rearranged and realigned differently during crack tip opening according to the network density.

Functionally graded fibrous scaffolds aim to replace sharp interfaces with gradual changes at the interface to prevent discontinuous material failure. Finite element analysis revealed that fracture of functionally graded networks can be controlled by tailoring the gradients of both network density and fiber alignment. Networks with fiber density gradients (DG) exhibit failure starting at the densest layer and show similar fracture toughness to homogeneous scaffolds. DAG networks featuring microstructural gradients in both density and fiber orientation over their thicknesses had improved fracture toughness as compared to DG networks. The DAG networks, which have aligned fibers at the densest network layer, postponed failure by rearranging and realigning the orientation of fibers from parallel to perpendicular to the notch to dissipate energy. The fiber rearrangement and realignment distributes stress instead of confining it within a small area [44]. This mechanism improves the fracture toughness of multilayer graded fibrous networks.

The current study has outlined experimental and computational methodologies for generating biomimetic functionally graded materials to recapitulate interface and connective tissues. In terms of mechanical properties, networks featuring both fiber density and alignment gradients are promising scaffold designs for these native tissues. One limitation in this work is that gelatin scaffolds require further crosslinking prior to use in biomedical applications, in order to prevent dissolution in aqueous media at physiological temperatures [45]. The degree of crosslinking and hydration of the construct will influence the ultimate scaffold mechanical properties [46], requiring further study of these factors on fracture behavior. In the future, we also plan to experimentally fabricate DAG networks based upon the computational models and compare their observed mechanical properties and fracture behavior to the simulations. We will also assess biocompatibility of the graded electrospun scaffolds, and observe how tailoring mechanical properties of the graded electrospun scaffolds affects cellular viability, ECM production and cell-scaffold interactions.

5. Conclusion

A trilayer scaffold with a microstructural architecture gradient has been successfully produced using a sequential electrospinning technique. The scaffold displayed a gradual increase in fiber diameter and pore size corresponding with a decrease in fiber packing densities from the bottom to top layer. Mechanical properties of both the functionally graded scaffolds and homogeneous scaffolds with fiber morphologies corresponding to that of each of the three layers of the graded scaffold were measured using uniaxial tensile and fracture tests. Mechanical properties of the homogeneous scaffolds, including elastic modulus, tensile strength, and fracture toughness, varied according to microstructural differences. This indicated that the mechanical properties of functionally graded electrospun scaffolds could be tailored by controlling the microstructure of the individual layers. This resulted in a gradual increase in modulus over the thickness of the graded scaffold, which led to the layer-by-layer crack propagation during fracture analysis. Finite element analysis of density-graded scaffolds indicated that fibers rearrange and deform differently at each network layer resulting in inhomogeneous strain distribution over the network thickness. Simulations of scaffolds combining gradients in both fiber density and alignment had larger crack tip openings before fracture, resulting in improved toughness. This work presents experimental methods of fabrication and computational methods of modeling the mechanical and fracture behavior of multilayer scaffolds. Consideration of the type and degree of gradient is critical for tailoring mechanical properties of the scaffold for specific applications. The methods presented herein can be used for the rational design of functionally graded multilayered fibrous scaffolds for interface and connective tissue engineering applications.

Acknowledgements

The authors would like to express their gratitude to Universiti Tun Hussein Onn Malaysia [Research Fund, UTHM], the Ministry of Energy, Science, Technology, Environment and Climate Change [IF1118C1042] and the Ministry of Education Malaysia [FRGS/1/2014/TK01/UTHM/02/2-1462] for funding the research work.

References

[1] N. Hasolli, Y.O. Park, Y.W. Rhee, Experimental study on filtration performance of flat sheet multiple-layer depth filter media for intake air filtration, Aerosol Sci. Technol. 47 (12) (2013) 1334–1341.
[2] Y. Yu, R. Ma, S. Yan, J. Fang, Preparation of multi-layer nylon-6 nanofibrous membranes by electrospinning and hot pressing methods for dye filtration, RSC Adv. 8 (22) (2018) 12173–12178.
[3] X. Tang, X. Yan, Multi-layer fibrous structures for noise reduction, The Journal of The Textile Institute 108 (12) (2017) 2096–2106.
[4] I.-N.E. Wang, S. Mitroo, F.H. Chen, H.H. Lu, S.B. Doty, Age-dependent changes in matrix composition and organization at the ligament-to-bone insertion, J. Orthop. Res. 24 (8) (2006) 1745–1755.
[5] L. Rossetti, L.A. Kuntz, E. Kunold, J. Schock, K.W. Müller, H. Grabmayr, J. Stolberg-Stolberg, F. Pfeiffer, S.A. Sieber, R. Burgkart, A.R. Bausch, The microstructure and micromechanics of the tendon-bone insertion, Nat. Mater. 16 (6) (2017) 664–670.
[6] I. Zizak, P. Roschger, O. Paris, B. Misof, A. Berzlanovich, S. Bernstorff, H. Amenitsch, K. Klaushofer, P. Fratzl, Characteristics of mineral particles in the human bone/cartilage interface, J. Struct. Biol. 141 (3) (2003) 208–217.
[7] G.M. Genin, A. Kent, V. Birman, B. Wopenka, J.D. Pasteris, P.J. Marquez, S. Thomopoulos, Functional grading of mineral and collagen in the attachment of tendon to bone, Biophys. J. 97 (4) (2009) 976–985.
[8] K.L. Moffat, W.-H.S. Sun, P.E. Pena, N.O. Chahine, S.B. Doty, G.A. Ateshian, C.T. Hung, H.H. Lu, Characterization of the structure-function relationship at the ligament-to-bone interface, Proc. Natl. Acad. Sci. 105 (23) (2008) 7947–7952.
[9] S. Thomopoulos, J.P. Marquez, B. Weinberger, V. Birman, G.M. Genin, Collagen fiber orientation at the tendon to bone insertion and its influence on stress concentrations, J. Biomech. 39 (10) (2006) 1842–1851.
[10] A. Changoor, M. Nelea, S. Méthot, N. Tran-Khanh, A. Chevrier, A. Restrepo, M.S. Shive, C.D. Hoemann, M.D. Buschmann, Structural characteristics of the collagen network in human normal, degraded and repair articular cartilages observed in polarized light and scanning electron microscopies, Osteoarthr. Cartil. 19 (12) (2011) 1458–1468.
[11] J.S. Bell, J. Christmas, J.C. Mansfield, R.M. Everson, C.P. Winlove, Micromechanical response of articular cartilage to tensile load measured using nonlinear microscopy, Acta Biomater. 10 (6) (2014) 2574–2581.
[12] S.L.Y. Woo, W.H. Akeson, G.F. Jemmott, Measurements of nonhomogeneous, directional mechanical properties of articular cartilage in tension, J. Biomech. 9 (12) (1976) 785–791.
[13] S.M. Bittner, B.T. Smith, L. Diaz-Gomez, C.D. Hudgins, A.J. Melchiorri, D.W. Scott, J.P. Fisher, A.G. Mikos, Fabrication and mechanical characterization of 3D printed vertical uniform and gradient scaffolds for bone and osteochondral tissue engineering, Acta Biomater. 90 (2019) 37–48.
[14] T.J. Levingstone, A. Ramesh, R.T. Brady, P.A.J. Brama, C. Kearney, J.P. Gleeson, F.J. O'Brien, Cell-free multi-layered collagen-based scaffolds demonstrate layer specific regeneration of functional osteochondral tissue in caprine joints, Biomaterials 87 (2016) 69–81.
[15] M.-H. Hong, H.J. Hong, H. Pang, H.-J. Lee, S. Yi, W.-G. Koh, Controlled release of growth factors from multilayered fibrous scaffold for functional recoveries in crushed sciatic nerve, ACS Biomaterials Science & Engineering 4 (2) (2018) 576–586.
[16] S.D. McCullen, H. Autefage, A. Callanan, E. Gentleman, M.M. Stevens, Anisotropic fibrous scaffolds for articular cartilage regeneration, Tissue Eng. A 18 (19–20) (2012) 2073–2083.
[17] T. Nie, L. Xue, M. Ge, H. Ma, J. Zhang, Fabrication of poly(L-lactic acid) tissue engineering scaffolds with precisely controlled gradient structure, Mater. Lett. 176 (2016) 25–28.
[18] J. Liu, L. Li, H. Suo, M. Yan, J. Yin, J. Fu, 3D printing of biomimetic multi-layered GelMA/nHA scaffold for osteochondral defect repair, Mater. Des. 171 (2019), 107708.
[19] H. Kang, Y. Zeng, S. Varghese, Functionally graded multilayer scaffolds for in vivo osteochondral tissue engineering, Acta Biomater. 78 (2018) 365–377.
[20] A. Di Luca, B. Ostrowska, I. Lorenzo-Moldero, A. Lepedda, W. Swieszkowski, C. Van Blitterswijk, L. Moroni, Gradients in pore size enhance the osteogenic

differentiation of human mesenchymal stromal cells in three-dimensional scaffolds, Sci. Rep. 6 (1) (2016), 22898.
[21] J.M. Sobral, S.G. Caridade, R.A. Sousa, J.F. Mano, R.L. Reis, Three-dimensional plotted scaffolds with controlled pore size gradients: effect of scaffold geometry on mechanical performance and cell seeding efficiency, Acta Biomater. 7 (3) (2011) 1009–1018.
[22] J. Nowlin, M.A. Bismi, B. Delpech, P. Dumas, Y. Zhou, G.Z. Tan, Engineering the hard–soft tissue interface with random-to-aligned nanofiber scaffolds, Nanobiomedicine 5 (2018), 184954351880353.
[23] J. Pu, K. Komvopoulos, Mechanical properties of electrospun bilayer fibrous membranes as potential scaffolds for tissue engineering, Acta Biomater. 10 (6) (2014) 2718–2726.
[24] C.P. Grey, S.T. Newton, G.L. Bowlin, T.W. Haas, D.G. Simpson, Gradient fiber electrospinning of layered scaffolds using controlled transitions in fiber diameter, Biomaterials 34 (21) (2013) 4993–5006.
[25] A.L. Butcher, C.T. Koh, M.L. Oyen, Systematic mechanical evaluation of electrospun gelatin meshes, J. Mech. Behav. Biomed. Mater. 69 (February) (2017) 412–419.
[26] W. Khoo, C.T. Koh, S.C. Lim, Synthetic and natural fibrous scaffolds for soft tissue engineering applications, J. Mech. Eng 4 (2017) 223–233.
[27] R. Mao, S. Goutianos, W. Tu, N. Meng, S. Chen, T. Peijs, Modelling the elastic properties of cellulose nanopaper, Mater. Des. 126 (2017) 183–189.
[28] C.T. Koh, M.L. Oyen, Branching toughens fibrous networks, J. Mech. Behav. Biomed. Mater. 12 (2012) 74–82.
[29] C.T. Koh, C.Y. Low, Y. Yusof, Structure-property relationship of bio-inspired fibrous materials, Procedia Computer Science 76 (2015) 411–416.
[30] M.A. Accardi, S.D. McCullen, A. Callanan, S. Chung, P.M. Cann, M.M. Stevens, D. Dini, Effects of fiber orientation on the frictional properties and damage of regenerative articular cartilage surfaces, Tissue Eng. A 19 (19–20) (2013) 2300–2310.
[31] Z. Chen, B. Wei, X. Mo, C.T. Lim, S. Ramakrishna, F. Cui, Mechanical properties of electrospun collagen–chitosan complex single fibers and membrane, Mater. Sci. Eng. C 29 (8) (2009) 2428–2435.
[32] H.H. Kim, M.J. Kim, S.J. Ryu, C.S. Ki, Y.H. Park, Effect of fiber diameter on surface morphology, mechanical property, and cell behavior of electrospun poly(ε-caprolactone) mat, Fibers and Polymers 17 (7) (2016) 1033–1042.
[33] C.T. Koh, M.L. Oyen, Toughening in electrospun fibrous scaffolds, APL Materials 3 (1) (2015), 014908.
[34] S.-C. Wong, A. Baji, S. Leng, Effect of fiber diameter on tensile properties of electrospun poly(ε-caprolactone), Polymer 49 (21) (2008) 4713–4722.
[35] C.A. Schneider, W.S. Rasband, K.W. Eliceiri, NIH Image to ImageJ: 25 years of image analysis, Nat. Methods 9 (7) (2012) 671–675.
[36] R.S. Rivlin, a.G. Thomas, Rupture of rubber. I. Characteristic energy for tearing, J. Polym. Sci. 10 (3) (1953) 291–318.
[37] C.T. Koh, D.G.T. Strange, K. Tonsomboon, M.L. Oyen, Failure mechanisms in fibrous scaffolds, Acta Biomater. 9 (7) (2013) 7326–7334.
[38] M.F. Kanninen, C.H. Popelar, Advanced Fracture Mechanics (No. 15), Oxford University Press, 1985.
[39] S. Gautam, A.K. Dinda, N.C. Mishra, Fabrication and characterization of PCL/gelatin composite nanofibrous scaffold for tissue engineering applications by electrospinning method, Mater. Sci. Eng. C 33 (3) (2013) 1228–1235.
[40] Y. Zhang, H. Ouyang, C.T. Lim, S. Ramakrishna, Z.-M. Huang, Electrospinning of gelatin fibers and gelatin/PCL composite fibrous scaffolds, J. Biomed. Mater. Res. 72B (1) (2005) 156–165.
[41] S. Soliman, S. Sant, J.W. Nichol, M. Khabiry, E. Traversa, A. Khademhosseini, Controlling the porosity of fibrous scaffolds by modulating the fiber diameter and packing density, Journal of Biomedical Materials Research - Part A 96 (*A*(3)) (2011) 566–574.
[42] F.J. O'Brien, B.A. Harley, M.A. Waller, I.V. Yannas, L.J. Gibson, P.J. Prendergast, The effect of pore size on permeability and cell attachment in collagen scaffolds for tissue engineering, Technology and Health Care: Official Journal of the European Society for Engineering and Medicine 15 (1) (2007) 3–17.
[43] T.B.F. Woodfield, C.A. Van Blitterswijk, J. De Wijn, T.J. Sims, A.P. Hollander, J. Riesle, Polymer scaffolds fabricated with pore-size gradients as a model for studying the zonal organization within tissue-engineered cartilage constructs, Tissue Eng. 11 (9–10) (2005) 1297–1311.
[44] U. Stachewicz, I. Peker, W. Tu, A.H. Barber, Stress delocalization in crack tolerant electrospun nanofiber networks, ACS Appl. Mater. Interfaces 3 (6) (2011) 1991–1996.
[45] Y.Z. Zhang, J. Venugopal, Z.M. Huang, C.T. Lim, S. Ramakrishna, Crosslinking of the electrospun gelatin nanofibers, Polymer 47 (8) (2006) 2911–2917.
[46] A. Bigi, G. Cojazzi, S. Panzavolta, K. Rubini, N. Roveri, Mechanical and thermal properties of gelatin films at different degrees of glutaraldehyde crosslinking, Biomaterials 22 (8) (2001) 763–768.